Journal of Power Sources 241 (2013) 12–19

Contents lists available at SciVerse ScienceDirect

Journal of Power Sources

journal homepage: www.elsevier.com/locate/jpowsour

Aging effects on high-temperature creep properties of a solid oxide fuel cell glass-ceramic sealant

Chih-Kuang Lin [a,*], Kun-Liang Lin [a], Jing-Hong Yeh [a], Wei-Hong Shiu [a], Chien-Kuo Liu [b], Ruey-Yi Lee [b]

[a] Department of Mechanical Engineering, National Central University, Jhong-Li 32001, Taiwan
[b] Physics Division, Institute of Nuclear Energy Research, Lung-Tan 32546, Taiwan

HIGHLIGHTS

- A longer thermal aging causes a higher crystallinity in GC-9 glass-ceramic sealant.
- Aged GC-9 has a greater flexural strength than the non-aged one at 800 °C.
- Non-aged GC-9 exhibits a much higher creep strain rate than the aged one at 800 °C.
- Creep stress exponent at 800 °C increases with thermal aging time for GC-9.
- A thermal aging of 1000 h significantly enhances creep resistance for GC-9.

ARTICLE INFO

Article history:
Received 30 January 2013
Received in revised form
19 April 2013
Accepted 21 April 2013
Available online 27 April 2013

Keywords:
Solid oxide fuel cell
Glass-ceramic sealant
High temperature
Creep property
Ring-on-ring test

ABSTRACT

Creep properties at 800 °C are investigated for a newly developed solid oxide fuel cell $BaO-B_2O_3-Al_2O_3-SiO_2$ glass-ceramic sealant (GC-9) in variously aged conditions using a ring-on-ring test technique. GC-9 specimens are thermally aged at 750 °C for 4 h (designated as non-aged), 100 h, or 1000 h after sintering at 850 °C. Results show a longer thermal aging treatment leads to a higher crystallinity and greater creep resistance for the given glass-ceramic sealant. When subjected to an applied constant load at 800 °C, the 1000 h-aged GC-9 lasts much longer than the non-aged and 100 h-aged ones before rupture. The 1000 h-aged GC-9 also exhibits a creep strain rate much smaller than that in the non-aged and 100 h-aged samples. The value of creep stress exponent increases from 6 to 29 as the aging treatment time is increased from 4 h to 1000 h. The creep strength at a rupture time of 1000 h for the non-aged, 100 h-aged, and 1000 h-aged GC-9 is about 21%, 28%, and 39%, respectively, of the corresponding Weibull characteristic strength at 800 °C.

© 2013 Elsevier B.V. All rights reserved.

1. Introduction

A solid oxide fuel cell (SOFC) is a highly efficient device for conversion of chemical energy directly into electrical power from a variety of fuels [1–3]. Among the SOFCs developed, planar SOFCs (pSOFCs) have a simple structural geometry, lower fabrication cost, and higher energy efficiency [4]. A pSOFC stack is a multi-layer structure consisting of repeated units of ceramic anode–electrolyte–cathode assembly and metallic components. The overall stack voltage is proportional to the number of cells in the stack. With a reduction in electrolyte thickness, progress has been made in pSOFCs to operate at an intermediate temperature range of 600 °C–800 °C to achieve lower material cost and to enhance component durability and stability [3]. The sealant is a critical material in a pSOFC stack to maintain its operation and performance. It is needed to bond components and form gas-tight seals to separate both the oxidant and fuel chambers. Match of coefficient of thermal expansion (CTE), chemical compatibility, and long-term durability are among the important characteristics for selecting a suitable sealant for a pSOFC stack.

Glass and glass-ceramics which have stable performance during high-temperature operation are currently a favorable candidate for sealing the components in pSOFCs [5,6]. In the glass and glass-ceramic systems developed for pSOFC, silicate glass systems with alkaline-earth modifiers are among the favorites because of their stable characteristics [5,6]. In addition, a self-healing feature of some glass systems has attracted more attention for pSOFC [7–17]. With suitable viscosity, a self-healing glass seal can restore its mechanical properties on being reheated to the stack operating temperature by healing the cooling-induced damages/cracks present at room temperature [11].

* Corresponding author. Tel.: +886 3 426 7340; fax: +886 3 425 4501.
E-mail address: t330014@cc.ncu.edu.tw (C.-K. Lin).

0378-7753/$ – see front matter © 2013 Elsevier B.V. All rights reserved.
http://dx.doi.org/10.1016/j.jpowsour.2013.04.088

The major sources of thermal stress in a pSOFC stack include mismatch of CTE and thermal gradient [18–20]. Under thermal cycling between steady-operation and shutdown stages, even a small CTE mismatch may give rise to significant thermal stresses in a pSOFC stack [18,19]. Although the stresses induced by thermal mismatch may not cause an immediate failure of pSOFC seals, they may generate creep deformation in the seals under a long-term high-temperature environment. Creep damages may eventually make seals deform excessively and even generate cracks. Gas leakage due to such creep damages would degrade cell performance and efficiency. From a design perspective, it is important to understand the long-term geometric stability and mechanical properties of glass/glass-ceramic sealants under the stack operating conditions so as to assess the structural integrity of a pSOFC stack. Therefore, a comprehensive high-temperature creep analysis of the glass/glass-ceramic seal is necessary for its successful application in pSOFCs.

There is limited work focused on the high-temperature creep properties of SOFC glass/glass-ceramic sealants in literature [10,13,21]. In those studies, short-term (less than 3 h) creep properties of a barium calcium alumino-silicate glass-ceramic sealant, G18, were investigated under a nanoindentation [13,21] or compression [10] loading condition. As a reliable pSOFC system is expected to operate stably at elevated temperature for a prolonged period of time (at least 20,000 h for commercial systems) and glass-ceramics are vulnerable to fracture under tensile stresses, more studies are needed to investigate the long-term creep properties of glass-ceramic sealants under a tensile loading mode. In addition, a glass sealant might crystallize during the assembling and operating stage of pSOFC to produce crystalline phases in the glass to become a glass-ceramic. After the crystallization process, thermal, chemical, and mechanical properties of a glass/glass-ceramic may be changed [22–26]. Such changes of material properties might influence its compatibility with other components, and the long-term stability and mechanical integrity of a pSOFC stack. A few studies [8–10,13,17,27–29] have investigated the complex crystallization effects on the mechanical properties and related mechanisms for sintered, powdered SOFC glasses. However, there is still lack of study for the crystallization effects on the long-term high-temperature creep behavior of SOFC glass-ceramic sealants.

Crystallization effects on the flexural strength and stiffness of a self-healing $BaO–B_2O_3–Al_2O_3–SiO_2$ glass (designated as GC-9) have been investigated for application in pSOFC [16,17]. As part of a series of studies on the high-temperature mechanical properties of glass/glass-ceramic sealants and metallic interconnects for pSOFCs [15–17,30–33], effects of thermal aging on the long-term high-temperature creep properties of the sintered GC-9 glass-ceramic sealant are investigated in the present study. Systematic constant-load ring-on-ring creep tests were conducted at 800 °C on variously aged GC-9 specimens to investigate the variation of creep behavior with crystalline phases. Such long-term high-temperature creep properties are important to the design of a reliable pSOFC stack and prediction of seal life.

2. Experimental procedures

2.1. Glass forming and specimen preparation

The GC-9 glass-ceramic sealant investigated in the study is a novel $BaO–B_2O_3–Al_2O_3–SiO_2$ glass which was developed by Institute of Nuclear Energy Research (INER) for application in pSOFCs [34–38]. It shows good thermal properties, chemical compatibility with other components, stability, and hermetic properties to be well used in pSOFCs [34–38]. Mechanical properties of GC-9 have been investigated at room temperature to 800 °C in both sintered and cast bulk forms in previous studies [15–17].

Major chemical composition of the patent GC-9 glass-ceramic includes 0–40 mol% BaO, 0–15 mol% B_2O_3, 0–10 mol% Al_2O_3, 0–40 mol% SiO_2, 0–15 mol% CaO, 0–15 mol% La_2O_3, and 0–5 mol% ZrO_2. The specific composition of the GC-9 glass-ceramic used in the current study is given elsewhere [39]. The given GC-9 glass-ceramic sealant was first made in a powder form. Details of the fabrication process of GC-9 powders were given elsewhere [17]. The GC-9 powders were then put into a mold and pressed to form a circular disk specimen with a diameter of 35 mm and thickness of 1.5 mm for ring-on-ring test. The GC-9 glass-ceramic disks were sintered at 850 °C for 4 h followed by aging at 750 °C for 4 h. Detailed heat-treatment steps during the sintering process can be found in a previous study [17]. Specimens through such heat-treatments are designated as non-aged GC-9 glass-ceramic. Although they are called non-aged GC-9 glass-ceramic, crystallization did take place in these specimens when sintered at 850 °C. Furthermore, in order to understand the effects of crystallization under a longer thermal aging on the creep properties of the sintered GC-9 glass-ceramic sealant, some specimens were also prepared by the same heat-treatment profile, except the aging time at 750 °C. These specimens were thermally aged at 750 °C for 100 h or 1000 h instead of 4 h. They are designated as 100 h-aged and 1000 h-aged GC-9 glass-ceramic, respectively. All of the specimens were polished with an 80-grit SiC paper to reduce surface roughness before creep testing. Crystalline phases in the variously aged GC-9 glass-ceramics were determined by X-ray diffraction (XRD). Scanning electron microscopy (SEM) with an energy dispersive X-ray spectrometer (EDS) was applied to analyze the microstructure and crystalline morphology.

2.2. Ring-on-ring creep test

Biaxial flexural test is a suitable method for determining the strength of plate-like materials because edge effects can be minimized. In the current work, a biaxial flexural ring-on-ring test of ASTM Standard C1499 [40] was applied to determine the mechanical and creep properties of the non-aged, 100 h-aged, and 1000 h-aged GC-9 specimens at 800 °C. Flexural strength of the non-aged and 100 h-aged GC-9 glass-ceramics at room temperature and 800 °C has been determined previously [17], while it was determined for the 1000 h-aged GC-9 in the current study using a similar ring-on-ring test technique described in Ref. [17].

Creep tests of variously aged GC-9 disk specimens were conducted under constant loading at 800 °C. Short-term creep tests were performed using a commercial closed-loop servo-hydraulic material test machine attached with a furnace. Long-term creep tests (>100 h) were conducted using a direct-load creep test machine. The flexural loading fixture with a 10-mm-diameter inner loading ring and a 20-mm-diameter outer supporting ring was made of alumina or nickel-based superalloy. Each specimen was heated to 800 °C at a heating rate of 6 °C min^{-1} and then held at 800 °C for 3 min before applying load. Several constant loadings were applied for each aged condition to obtain the creep strain–time and stress–rupture time relationships.

According to ASTM Standard C1499 [40], the formula for calculating the biaxial flexural stress, σ, of a thin circular plate is given as

$$\sigma = \frac{3P}{2\pi h^2}\left[(1-\nu)\frac{D_S^2 - D_L^2}{2D^2} + (1+\nu)\ln\frac{D_S}{D_L}\right] \quad (1)$$

where P is the applied force, h is thickness of the specimen, and D_L, D_S, and D are diameters of the load ring, support ring, and specimen, respectively. In the present study, Poisson's ratio $\nu = 0.3$ is used in Eq. (1). Deflection contour in the thickness direction from

center to edge of the specimen was derived in a previous study [41] and is given as

$$\delta = \frac{3P(1-\nu^2)R_L^2}{2\pi h^3 E}\left\{\left(\frac{R_S}{R_L}\right)^2 - 1 - \left[\left(\frac{R}{R_L}\right)^2 + 1\right]\ln\left(\frac{R_S}{R_L}\right) + \frac{1}{2}\frac{1-\nu}{1+\nu}\frac{R_S^2 - R_L^2}{R_{SP}^2}\frac{R_S^2 - R^2}{R_L^2}\right\} \quad \text{for } 0 \le R \le R_L \tag{2}$$

where δ is the deflection of specimen at a specified point, E is the Young's modulus of specimen, R is the radial distance from disk center to the specified point, and R_L, R_S, and R_{SP} are radii of the load ring, support ring, and specimen, respectively. In the present study, vertical displacement of the actuator in the servo-hydraulic material test machine and vertical displacement of the loading rod in the direct-load creep test machine both were measured. Such a displacement is regarded as deflection of the specimen at the contact point in the inner loading ring ($R = R_L$). The biaxial flexural strain in a plane stress condition can be determined as follows,

$$\varepsilon = (1-\nu)\frac{\sigma}{E} \tag{3}$$

Substitution of Eqs. (1) and (2) with $R = R_L$ into Eq. (3) yields

$$\varepsilon = \frac{(1-\nu)h\delta}{R_L^2}\left\{\frac{(1-\nu)\dfrac{R_S^2 - R_L^2}{R_{SP}^2} + (1+\nu)\ln\dfrac{R_S}{R_L}}{\left(\dfrac{R_S}{R_L}\right)^2 - 1 - 2\ln\left(\dfrac{R_S}{R_L}\right) + \dfrac{1}{2}\dfrac{1-\nu}{1+\nu}\dfrac{R_S^2 - R_L^2}{R_{SP}^2}\dfrac{R_S^2 - R_L^2}{R_L^2}}\right\} \tag{4}$$

During a creep test, the measured actuator (or loading rod) displacement δ varies with time. Accordingly, the apparent creep strain–time relationship in a ring-on-ring creep test can be obtained through Eq. (4) with variation of time.

3. Results and discussion

3.1. Microstructure and flexural strength

SEM micrographs in back-scattered electron (BSE) mode for variously aged GC-9 glass-ceramics are shown in Fig. 1. Darker gray needles, which are the primary crystalline phase, alpha-Ba($Al_2Si_2O_8$), are clearly observed in all of the given three aged conditions (Fig. 1). Microvoids (the darkest phase) are also found in Fig. 1 for variously aged GC-9 as a result of burning of binder and/or plasticizer during sintering process. They might even be formed during cooling step due to CTE mismatch between the crystalline phases and residual glass in the GC-9 glass-ceramic. In addition to the alpha-Ba($Al_2Si_2O_8$) phase, other minor crystalline phases are also detected in the given GC-9 glass-ceramics. Fig. 2 shows the XRD patterns of GC-9 in variously aged conditions. Note that in Fig. 2 only the peaks higher than a certain level of intensity are labeled for each phase to avoid confusion with too many symbols. A comprehensive list of peaks observed for each phase is given in Table 1. As shown in Fig. 2, phase peaks for alpha-Ba($Al_2Si_2O_8$) are detected in each given aged condition. In the non-aged and 100 h-aged GC-9 glass-ceramics, $BaSiO_3$ and $Ba_3La_6(SiO_4)_6$ crystalline phases are also detected (Fig. 2). In the 1000 h-aged GC-9 glass-ceramic, crystalline phases $Ca(Al_2Si_2O_8)$ and Al_2SiO_5 are also detected, but phase peaks for $BaSiO_3$ and $Ba_3La_6(SiO_4)_6$ disappear (Fig. 2). As expected, crystallinity increases with thermal aging time and alpha-Ba($Al_2Si_2O_8$) remains the primary crystalline phase in aged GC-9. The amount and size of the needle alpha-Ba($Al_2Si_2O_8$) phases in a further aged GC-9 are greater than those in the non-aged GC-9, as shown in Fig. 1. The amount of the main crystalline phase, alpha-Ba($Al_2Si_2O_8$), is estimated by calculating the average area proportion of the darker gray needles in ten SEM micrographs for each aged condition. As a result, the area proportion of the crystalline alpha-Ba($Al_2Si_2O_8$) phase is approximately 18%, 37%, and 43%, in the non-aged, 100 h-aged, and 1000 h-aged GC-9, respectively.

Weibull statistics [42] is commonly used to describe the fracture behavior of brittle materials. Using a similar Weibull analysis method described in Ref. [17], the two-parameter Weibull distribution of flexural strength for the given GC-9 glass-ceramics at room temperature and 800 °C is shown in Fig. 3. Note in Fig. 3 F is the failure probability for an applied stress σ. Table 2 lists the Weibull characteristic strength σ_0 (corresponding to $F = 63.2\%$) and Weibull modulus m for the non-aged, 100 h-aged, and 1000 h-aged GC-9 glass-ceramics at each testing temperature. As shown in Table 2, flexural strength of the 1000 h-aged and 100 h-aged GC-9 at 800 °C is about twice that of the non-aged one. As shown in Fig. 3, the 1000 h-aged condition always has the greatest flexural strength at each testing temperature. This is attributable to a greater extent of crystallization through a longer thermal aging treatment. Generally, crystalline phases in the glass and glass-ceramic can enhance mechanical strength. All of the non-aged, 100 h-aged, and 1000 h-aged GC-9 crystallize and become glass-ceramic after the given sintering process and thermal aging treatment. It has been reported the glass transition temperature of GC-9 is increased with a longer thermal aging time and a higher crystallinity [17]. As expected, a larger amount of crystalline phases in the 1000 h-aged GC-9 glass-ceramic strengthen the high-temperature mechanical strength to a greater extent compared to the non-aged and 100 h-aged ones.

In mechanical failure of a brittle material, the Weibull modulus m is related to the shape, size, and distribution of strength-controlling flaws. A higher value of m indicates a less scattering in strength data and a smaller range of distribution in flaw size and shape. As shown in Table 2, the Weibull moduli for the given three aged conditions are comparable at 800 °C. At room temperature, the non-aged condition has a m value lower than that of the two aged conditions. Apparently, outlines of the surface defects in the given three aged conditions at 800 °C are modified to a more consistent form due to a crack healing effect [15–17]. Although characteristics of the surface defects are comparable at 800 °C for the given three aged conditions, the differential flexural strength values at 800 °C indicate crystallinity plays a major role in determining the high-temperature mechanical properties for the given GC-9 glass-ceramic sealant.

3.2. Creep deformation

In a typical creep strain versus time curve, there is an initial instantaneous response of elastic and perhaps plastic strain, then followed by a gradual accumulation of creep strain. In the primary stage, strain rate is relatively high at beginning. However, strain rate decreases to a minimum due to work hardening when the primary stage is ended [43]. The second stage having a near constant strain rate is called steady-state creep [43]. At the end of the secondary stage, strain rate increases again in an unstable manner as rupture failure approaches. Creep damages forming inside the material accumulate to a certain extent and cause rupture in the tertiary stage [43].

Fig. 4 shows typical variations of apparent strain with time for the non-aged, 100 h-aged, and 1000 h-aged GC-9 tested at 800 °C. As shown in Fig. 4, a larger loading causes a shorter creep rupture

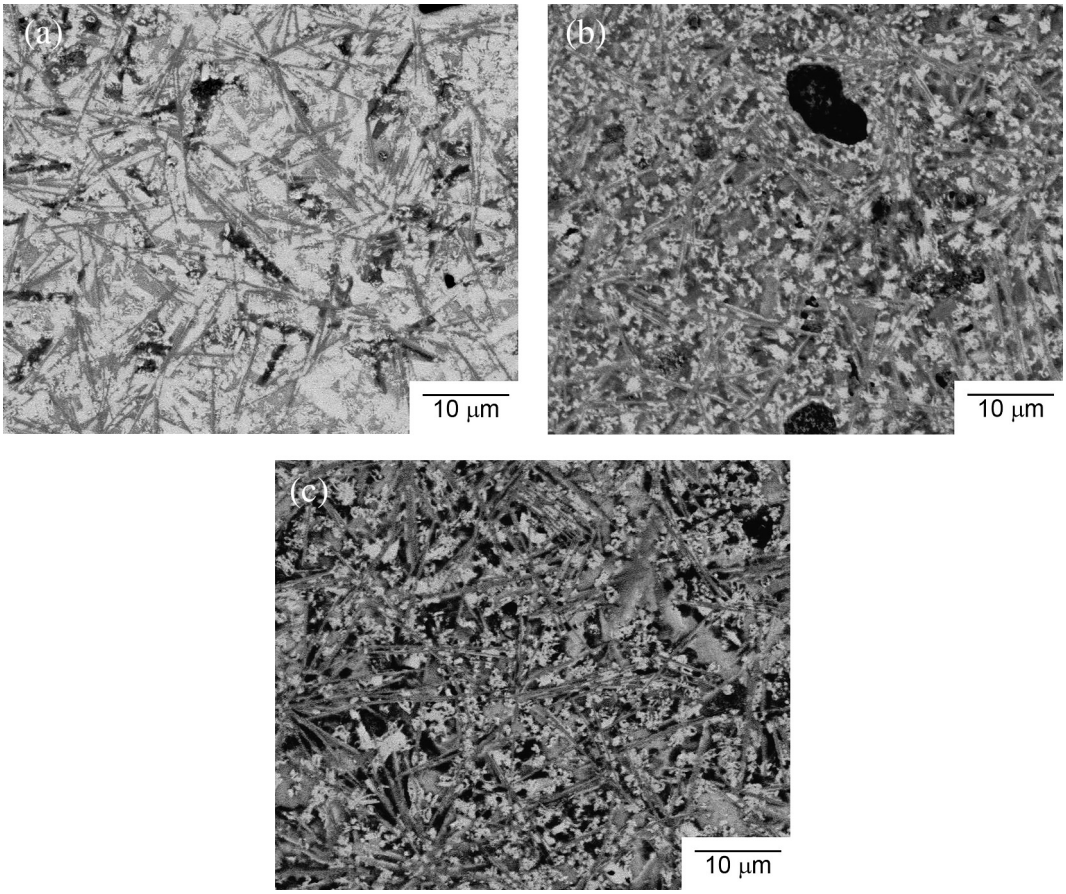

Fig. 1. SEM micrographs (in BSE mode) of variously aged GC-9 glass-ceramics: (a) non-aged; (b) 100 h-aged; (c) 1000 h-aged.

time. For the non-aged GC-9, the applied constant loads are in the range of 30 N–70 N. The corresponding apparent stresses applied are equal to 6 MPa–13 MPa based on Eq. (1). For an applied apparent stress of 13 MPa or 11 MPa, the creep rupture time is less than 1 h and no steady-state creep is observed, as shown in Fig. 4(a). Under a smaller stress such as 8 MPa or 10 MPa, a secondary stage is observed and followed by an inflection point and the tertiary stage, as shown in Fig. 4(a) and (b). In contrast, the tertiary stage disappears in some low-stress cases. For example, the 6-MPa creep curve (Fig. 4(b)) shows a long-term secondary stage without a tertiary stage. For the long-term 6-MPa curve, strain rate decreases initially and becomes near constant after the primary stage. This is due to a balance between work hardening and thermal/viscous softening.

As described above, a greater flexural strength of the aged GC-9 over the non-aged one is observed at 800 °C due to a greater extent of crystallization. Therefore, the applied constant loads are slightly increased for the aged GC-9 to reach a certain equivalent rupture time. As shown in Fig. 4(c), for an apparent stress of 11 MPa or above, the creep rupture time of the 100-h aged GC-9 is less than 10 h with no noticeable secondary stage of creep deformation. Steady-state creep deformation is observed for an apparent stress of 10 MPa or below, and the creep rupture time is in the range of

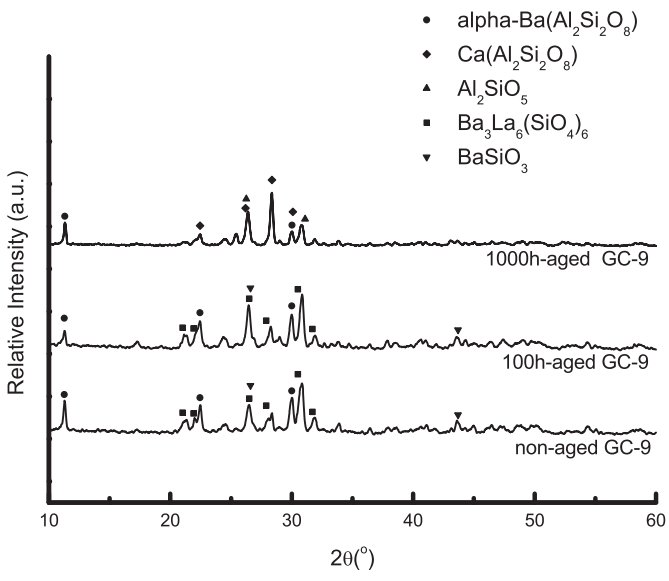

Fig. 2. XRD patterns of GC-9 glass-ceramic in variously aged conditions.

Table 1
Angles of XRD peaks observed for each crystalline phase in variously aged GC-9 glass-ceramics.

Phase	2θ (°)
Alpha-Ba($Al_2Si_2O_8$)	11.35, 19.34, 22.48, 22.82, 30.08, 33.82, 46.61
Ca($Al_2Si_2O_8$)	22.41, 26.21, 28.31, 28.43, 29.97, 31.55, 31.72
Al_2SiO_5	26.24, 26.6, 28.05, 30.55, 30.87, 31.05, 43.05
$Ba_3La_6(SiO_4)_6$	20.94, 21.82, 24.3, 26.50, 27.82, 30.47, 31.63
$BaSiO_3$	24.43, 26.59, 29.06, 32.07, 33.67, 40.9, 43.7

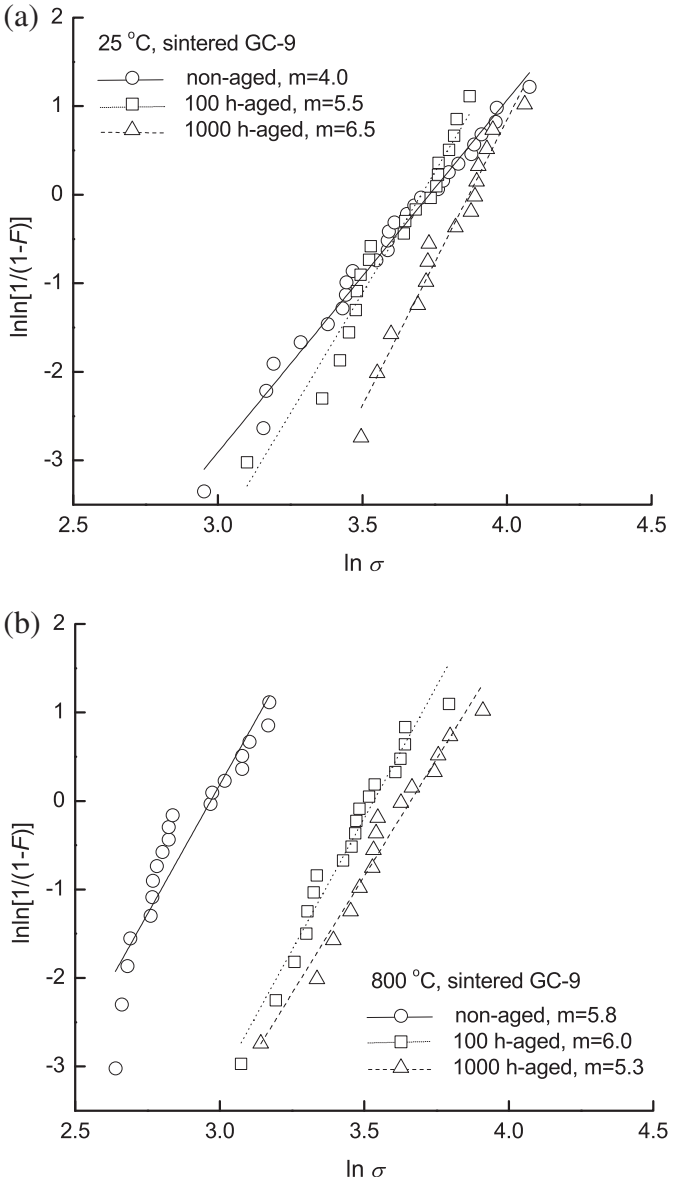

Fig. 3. Weibull distribution of flexural strength for variously aged GC-9 glass-ceramics: (a) at room temperature; (b) at 800 °C. (σ is in unit of MPa. Data of the non-aged and 100 h-aged GC-9 are taken from Ref. [17].)

hundreds to thousands of hours for the 100 h-aged GC-9, as shown in Fig. 4(d). For an apparent stress of 9 MPa, the 100 h-aged specimen exhibits a long-term secondary creep and runs out without rupture at a time longer than 1000 h (Fig. 4(d)). Similarly, a long-term secondary stage is present but at a higher stress of 15 MPa for the 1000 h-aged GC9, as shown in Fig. 4(f).

Table 2
Weibull characteristic strength (σ_0) and Weibull modulus (m) for variously aged GC-9 glass-ceramics at different temperatures.

	Aged condition	Temperature	
		25 °C	800 °C
σ_0 (MPa)	Non-aged	42	19
	100 h-aged	41	34
	1000 h-aged	49	38
m	Non-aged	4	5.8
	100 h-aged	5.5	6
	1000 h-aged	6.5	5.3

Data of the non-aged and 100 h-aged conditions are taken from Ref. [17].

As the 1000 h-aged GC-9 contains a larger amount of crystalline phases, it exhibits a greater flexural strength and creep resistance as compared to the non-aged and 100 h-aged ones. Fig. 5 shows a comparison of creep strain curves in the first 10 h of variously aged GC-9 under an apparent stress of 15 MPa or 13 MPa. As the loading level of 15 MP is not applied in the non-aged GC-9, the highest apparent stress 13 MPa is selected instead for comparison in Fig. 5. Rupture of the non-aged and 100 h-aged GC-9 specimens occurs at a time less than 1 h, as shown in Fig. 5. For the 1000 h-aged GC-9 specimen, it shows a long-term secondary creep without rupture when the test time exceeds 1000 h. A rapid, large deformation in the non-aged GC-9 is caused by a larger amount of amorphous glass phase. The creep strain does not have a drastic increase for the 1000 h-aged GC-9 before entering into the secondary stage. For a given loading of 15 MPa, the creep strain curve of the 1000 h-aged GC-9 exhibits a slope much smaller than that of the 100 h-aged one (Fig. 5). As the crystalline phases have a higher glass transition temperature and a greater stiffness, they would retard flow of the residual glass phase at 800 °C in the given GC-9 glass-ceramic sealant. In this regard, a much smaller creep deformation is found for the 1000 h-aged GC-9 which has the largest content of crystalline phases among the given three aged conditions. Therefore, as expected, GC-9 having a higher crystallinity is more resistant to creep at 800 °C.

Analysis of creep deformation is usually related to the secondary stage. The Norton relationship is most often used for creep deformation analysis. The Norton's power law [43] which is used to correlate the minimum creep strain rate with applied stress at a given temperature for a material is expressed as below,

$$\dot{\varepsilon}_{\min} = A\sigma^n \tag{5}$$

where $\dot{\varepsilon}_{\min}$ is the minimum creep strain rate, A is a material constant, σ is the applied stress, and n is the stress exponent. The stress exponent (n) depends on the creep deformation mechanism acting during a creep test. For a creep mechanism due to viscous flow in amorphous solids such as silica glass and some polymers, n is equal to 1. A value of n in the range of 3–10 (typically around 5) represents a dislocation type of creep mechanism for crystalline metals and ceramics [44]. Dislocation creep, also called power-law creep, involves a more drastic motion of dislocations which are vacancies or some defects [43].

Fig. 6 shows the relationship between minimum creep strain rate and applied apparent stress for variously aged GC-9 at 800 °C. The fitted equation and correlation coefficient (r) for each curve in Fig. 6 are given as follows,

$$\text{Non}-\text{aged}: \quad \dot{\varepsilon}_{\min} = 6.59\times10^{-12}\sigma^{5.59}, \quad r^2 = 0.64 \tag{6}$$

$$100\text{ h}-\text{aged}: \quad \dot{\varepsilon}_{\min} = 3.41\times10^{-25}\sigma^{16.47}, \quad r^2 = 0.94 \tag{7}$$

$$1000\text{ h}-\text{aged}: \quad \dot{\varepsilon}_{\min} = 9.91\times10^{-44}\sigma^{28.69}, \quad r^2 = 0.96 \tag{8}$$

where $\dot{\varepsilon}_{\min}$ is the minimum creep strain rate in unit of s^{-1} and σ is the applied apparent stress in unit of MPa. As shown in Fig. 6, the non-aged GC-9 exhibits a higher minimum strain rate than do the 100 h-aged and 1000 h-aged ones given an apparent stress. The values of n are around 6, 16, and 29 for the non-aged, 100 h-aged, and 1000 h-aged GC-9, respectively. Because of existence of crystalline phases in the given three aged conditions, the stress exponent does not show a value of $n = 1$ for viscous creep in amorphous glass. The obtained n values indicate a possible power-law

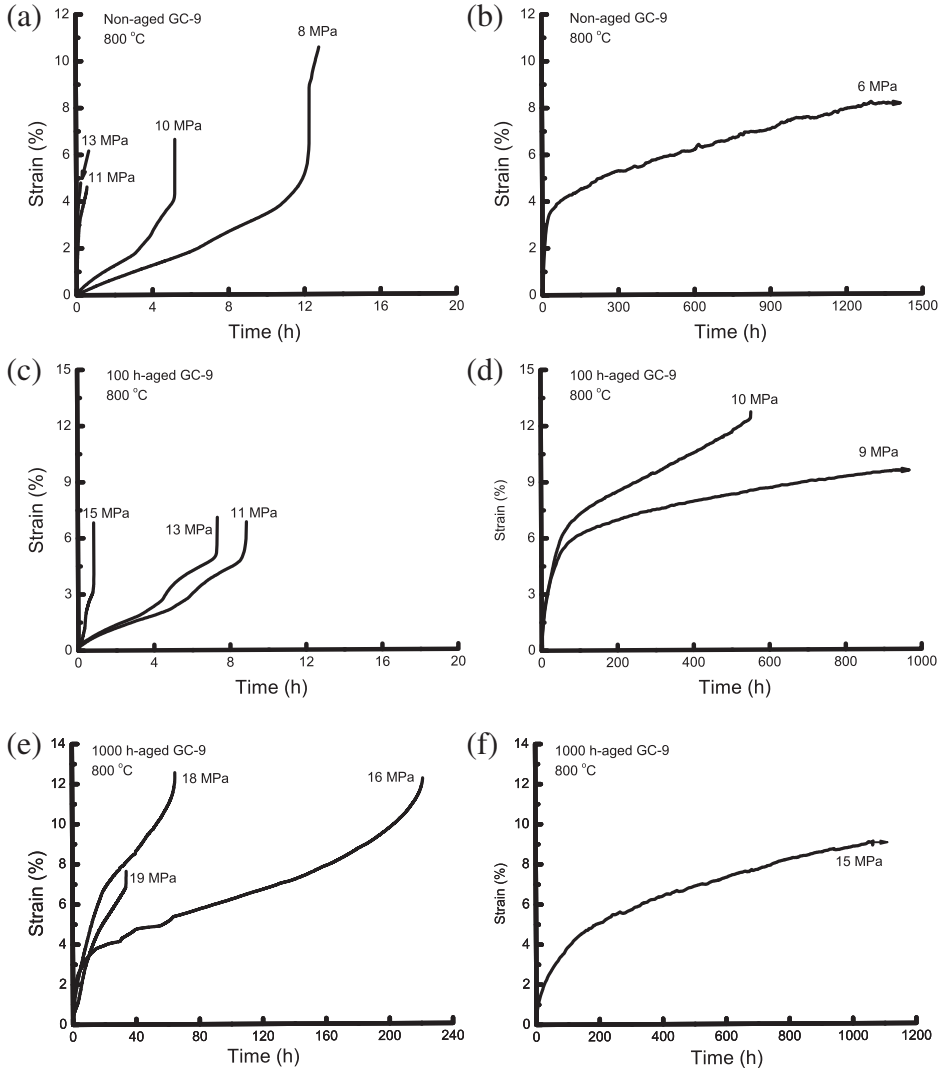

Fig. 4. Typical creep strain curves for variously aged GC-9 glass-ceramics at 800 °C: (a) short-term for non-aged; (b) long-term for non-aged; (c) short-term for 100 h-aged; (d) mid/long-term for 100 h-aged; (e) short/mid-term for 1000 h-aged; (f) long-term for 1000 h-aged. (Arrows indicate the specimens were not ruptured when the test was terminated.)

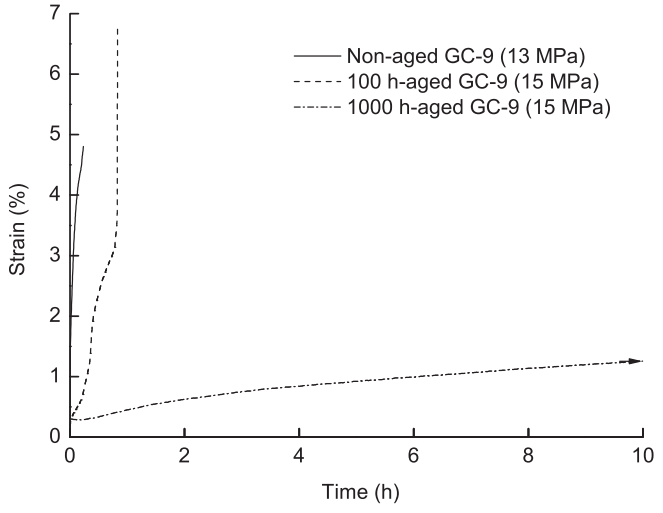

Fig. 5. Typical creep strain curves in the first 10 h for variously aged GC-9 glass-ceramics under an apparent stress of 13 MPa or 15 MPa. (Arrow indicates the specimen was not ruptured within the first 10 h.)

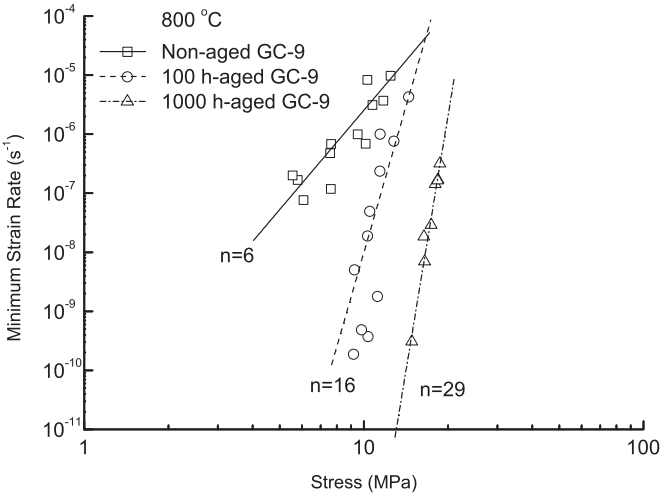

Fig. 6. Relationship between minimum creep strain rate and applied apparent stress for variously aged GC-9 glass-ceramics at 800 °C.

dislocation creep mechanism at 800 °C for the variously aged GC-9 glass-ceramics. Nevertheless, the stress exponent for the 100 h-aged and 1000 h-aged GC9 ($n = 16$ and 29, respectively) is much higher than the typical value of dislocation creep mechanism for crystalline metals and ceramics ($3 < n < 10$). In addition, a greater stress exponent value is found for a longer thermal aging accompanied with a greater extent of crystallization. It is not clear at present whether there is any other creep mechanism involved in the high n values of the 100 h-aged and 1000 h-aged GC-9, in addition to the power-law dislocation mechanism.

3.3. Creep life

Fig. 7 shows the relationship between the applied apparent stress and creep rupture time at 800 °C for variously aged GC-9. As shown in Fig. 7, the creep rupture time for a given aged condition generally increases with a decrease in applied loading. The relationship between the applied apparent stress and creep rupture time can be described by a simple power law for each aged condition. The fitted equation and correlation coefficient (r) for each curve in Fig. 7 are expressed as follows,

$$\text{Non} - \text{aged}: \quad \sigma t_r^{0.14} = 10.54, \quad r^2 = 0.79 \tag{9}$$

$$100\text{ h} - \text{aged}: \quad \sigma t_r^{0.051} = 13.49, \quad r^2 = 0.68 \tag{10}$$

$$1000\text{ h} - \text{aged}: \quad \sigma t_r^{0.057} = 21.91, \quad r^2 = 0.63 \tag{11}$$

where σ is the applied apparent stress in unit of MPa and t_r is time to rupture in unit of h. The creep rupture time at 800 °C for variously aged GC-9 can be estimated through these power-law relations. As shown in Fig. 7, slope of the curve for the non-aged GC-9 is steeper than that of the 100 h-aged and 1000 h-aged ones.

As shown in Fig. 7, given an apparent stress, the creep rupture time for the given three aged conditions takes the following order: 1000 h-aged > 100 h-aged > non-aged. According to Eq. (9), the creep strength corresponding to a rupture time of 1000 h is 4 MPa for the non-aged GC-9. For the 100 h-aged and 1000 h-aged GC-9, the creep strength at a rupture time of 1000 h is estimated to be 9.5 MPa and 14.8 MPa, respectively, based on Eqs. (10) and (11). As listed in Table 1, the Weibull characteristic strength at 800 °C for the non-aged, 100 h-aged, and 1000 h-aged GC-9 is 19 MPa, 34 MPa, and 38 MPa, respectively. Therefore, the creep strength at a rupture time of 1000 h for the non-aged, 100 h-aged, and 1000 h-aged GC-9 is about 21%, 28%, and 39%, respectively, of the corresponding Weibull characteristic strength. Apparently, a 1000-h thermal aging treatment significantly enhances the creep strength of GC-9 glass-ceramic sealant at 800 °C due to a greater crystallinity.

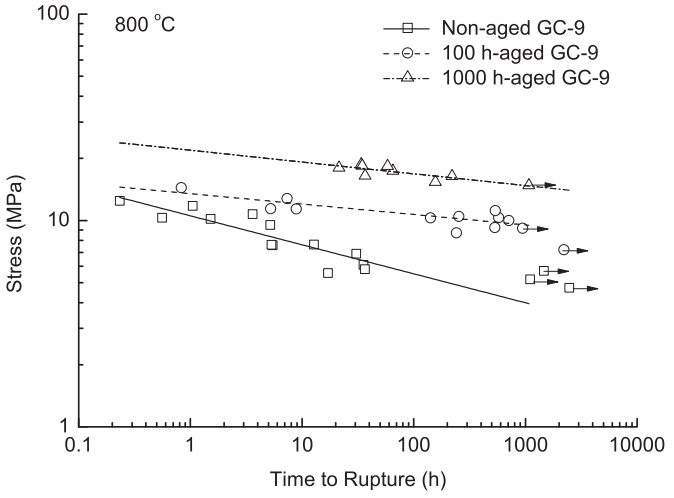

Fig. 7. Applied apparent stress versus rupture time for variously aged GC-9 glass-ceramics. (Arrows indicate the specimens were not ruptured when the test was terminated.)

When the applied constant load is reduced to 30 N (6 MPa) for the non-aged GC-9, it shows a dual behavior in creep rupture time (Fig. 7). Some specimens fail at a time less than 30 h, while others last longer than 1000 h. Such a scattering in creep rupture time might be attributed to an in-situ aging/crystallization mechanism acting in the non-aged GC-9 during creep test. The in-situ crystallization increases the crystallinity of the non-aged GC-9 to a certain extent resulting in a greater creep resistance, if the specimen survives the first 30 h.

4. Conclusions

(1) The crystallinity in GC-9 glass-ceramic sealant is increased with thermal aging time. The apparent content of the major crystalline alpha-Ba($Al_2Si_2O_8$) phase is approximately 18%, 37%, and 43%, in the non-aged, 100 h-aged, and 1000 h-aged GC-9, respectively. The 1000 h-aged GC-9 has a greater flexural strength than do the non-aged and 100 h-aged ones at both room temperature and 800 °C, due to a higher crystallinity.

(2) Given an applied constant load, the creep rupture time of the 1000 h-aged GC-9 at 800 °C is much longer than that of the non-aged and 100 h-aged ones. The non-aged GC-9 exhibits a higher creep strain rate than do the 100 h-aged and 1000 h-aged ones. Therefore, the GC-9 having a higher crystallinity is more resistant to creep at 800 °C.

(3) The values of creep stress exponent (n) are of 6, 16, and 29 for the non-aged, 100 h-aged, and 1000 h-aged GC-9, respectively. The GC-9 glass-ceramic sealant with a longer thermal aging and a greater extent of crystallization exhibits a higher creep stress exponent value.

(4) If the creep rupture time at 800 °C needs to be longer than 1000 h for the non-aged, 100 h-aged, and 1000 h-aged GC-9, the applied apparent stress should be less than 4 MPa, 9.5 MPa, and 14.8 MPa, respectively.

Acknowledgment

This work was supported by the National Science Council (Taiwan) under Contract No. NSC 95-2221-E-008-004-MY3 and by the Institute of Nuclear Energy Research (Taiwan) under Contract No. 1002001INER053.

References

[1] M.A.J. Cropper, S. Geiger, D.M. Jollie, J. Power Sources 131 (2004) 57–61.
[2] N.Q. Minh, Solid State Ion. 171 (2004) 271–277.
[3] A. Weber, E. Ivers-Tiffée, J. Power Sources 127 (2004) 273–283.
[4] I. Antepara, I. Villarreal, L.M. Rodriguez-Martinez, N. Lecanda, U. Castro, A. Laresgoiti, J. Power Sources 151 (2005) 103–107.
[5] J.W. Fergus, J. Power Sources 147 (2005) 46–57.
[6] P.A. Lessing, J. Mater. Sci. 42 (2007) 3465–3476.
[7] R.N. Singh, Int. J. Appl. Ceram. Technol. 4 (2007) 134–144.
[8] K.D. Meinhardt, D.-S. Kim, Y.-S. Chou, K.S. Weil, J. Power Sources 182 (2008) 188–196.
[9] N. Govindaraju, W.N. Liu, X. Sun, P. Singh, R.N. Singh, J. Power Sources 190 (2009) 476–484.
[10] E.V. Stephens, J.S. Vetrano, B.J. Koeppel, Y. Chou, X. Sun, M.A. Khaleel, J. Power Sources 193 (2009) 625–631.
[11] W.N. Liu, X. Sun, B. Koeppel, M.A. Khaleel, Int. J. Appl. Ceram. Technol. 7 (2010) 22–29.
[12] W.N. Liu, X. Sun, M.A. Khaleel, J. Power Sources 196 (2011) 1750–1761.

[13] J. Milhans, D.S. Li, M. Khaleel, X. Sun, M.S. Al-Haik, A. Harris, H. Garmestani, J. Power Sources 196 (2011) 5599–5603.
[14] W. Xu, X. Sun, E. Stephens, I. Mastorakos, M.A. Khaleel, H. Zbib, J. Power Sources 218 (2012) 445–454.
[15] H.-T. Chang, C.-K. Lin, C.-K. Liu, J. Power Sources 189 (2009) 1093–1099.
[16] H.-T. Chang, C.-K. Lin, C.-K. Liu, J. Power Sources 195 (2010) 3159–3165.
[17] H.-T. Chang, C.-K. Lin, C.-K. Liu, S.-H. Wu, J. Power Sources 196 (2011) 3583–3591.
[18] C.-K. Lin, T.-T. Chen, Y.-P. Chyou, L.-K. Chiang, J. Power Sources 164 (2007) 238–251.
[19] C.-K. Lin, L.-H. Huang, L.-K. Chiang, Y.-P. Chyou, J. Power Sources 192 (2009) 515–524.
[20] L. Blum, S.M. Gross, J. Malzbender, U. Pabst, M. Peksen, R. Peters, I.V. Vinke, J. Power Sources 196 (2011) 7175–7181.
[21] J. Milhans, M. Khaleel, X. Sun, M. Tehrani, M. Al-Haik, H. Garmestani, J. Power Sources 195 (2010) 3631–3635.
[22] Z. Strnad, Glass-Ceramic Materials, Elsevier Science Publishing Company, Inc., New York, USA, 1986.
[23] D.G. Burnett, R.W. Douglas, Discuss. Faraday Soc. 50 (1970) 200–205.
[24] D.G. Burnett, R.W. Douglas, Phys. Chem. Glasses 12 (1971) 117–124.
[25] J.E. Shelby, Introduction to Glass Science and Technology, second ed., Royal Society of Chemistry, New York, USA, 2005.
[26] R. Hill, P. Gilbert, J. Am. Ceram. Soc. 76 (1993) 417–425.
[27] Y. Zhao, J. Malzbender, S.M. Gross, J. Eur. Ceram. Soc. 31 (2011) 541–548.
[28] J. Malzbender, Y. Zhao, J. Mater. Sci. 47 (2012) 4342–4347.
[29] W. Liu, X. Sun, M.A. Khaleel, J. Power Sources 185 (2008) 1193–1200.
[30] Y.-T. Chiu, C.-K. Lin, J.-C. Wu, J. Power Sources 196 (2011) 2005–2012.
[31] Y.-T. Chiu, C.-K. Lin, J. Power Sources 198 (2012) 149–157.
[32] C.-K. Lin, J.-Y. Chen, J.-W. Tian, L.-K. Chiang, S.-H. Wu, J. Power Sources 205 (2012) 307–317.
[33] Y.-T. Chiu, C.-K. Lin, J. Power Sources 219 (2012) 112–119.
[34] C.-K. Liu, T.-Y. Yung, K.-F. Lin, in: Proceedings of the Annual Conference of the Chinese Ceramic Society 2007 (CD-ROM), 2007 (in Chinese).
[35] C.-K. Liu, T.-Y. Yung, S.-H. Wu, K.-F. Lin, in: Proceedings of the MRS_Taiwan Annual Meeting 2007 (CD-ROM), 2007 (in Chinese).
[36] C.-K. Liu, T.-Y. Yung, K.-F. Lin, in: Proceedings of the Annual Conference of the Chinese Ceramic Society 2008 (CD-ROM), 2008 (in Chinese).
[37] C.-K. Liu, K.-C. Tsai, K. F. Lin, S.-H. Wu, T.-Y. Yung, in: Proceedings of the Annual Conference of the Chinese Ceramic Society 2009 (CD-ROM), 2009 (in Chinese).
[38] C.-K. Liu, T.-Y. Yung, K.-F. Lin, R.-Y. Lee, S.-H. Wu, ECS Trans. 25 (2009) 1491–1500.
[39] C.-K. Liu, T.-Y. Yung, K.-F. Lin, R.-Y. Lee, T.-S. Lee, Glass-Ceramic Sealant for Planar Solid Oxide Fuel Cells, United States Patent No. 7,897,530 B2, 2011.
[40] ASTM Standard C1499-08, Standard Test Method for Monotonic Equibiaxial Flexural Strength of Advanced Ceramics at Ambient Temperature, ASTM International, West Conshohocken, PA, USA, 2008.
[41] R.W. Schmitt, K. Blank, G. Schönbrunn, Sprechsaal 116 (1983) 397–409 (in German).
[42] D.W. Richerson, Modern Ceramic Engineering, second ed., Marcel Dekker, Inc., New York, USA, 1992.
[43] N.E. Dowling, Mechanical Behavior of Materials: Engineering Methods for Deformation, Fracture, and Fatigue, third ed., Pearson Education, Inc., New Jersey, USA, 2007.
[44] H.J. Frost, M.F. Ashby, Deformation-Mechanism Maps: The Plasticity and Creep of Metals and Ceramics, Pergamon Press, Oxford, UK, 1982.